Title

TOUGH2-seed: A coupled fluid flow and mechanical-stochastic approach to model injection-induced seismicity

Authors

Rinaldi, Antonio P
Nespoli, Massimo

Publication Date

2017-11-01

DOI

10.1016/j.cageo.2016.12.003

Peer reviewed

TOUGH2-seed: A coupled fluid flow and mechanical-stochastic approach to model injection-induced seismicity

Antonio P. Rinaldi[a], Massimo Nespoli[bc]
[a]Swiss Seismological Service, Swiss Federal Institute of Technology, ETHZ, Zürich, Switzerland
[b]Istituto Nazionale di Geofisica e Vulcanologia, Sezione di Bologna, Italy
[c]Department of Physics and Astronomy, University of Bologna, Italy

Abstract

Understanding the injection-induced triggering mechanism is a fundamental step towards controlling the seismicity generated by deep underground exploitation. Here we propose a modeling approach based on coupling the TOUGH2 simulator with a geomechanical-stochastic model. The hydro-mechanical-stochastic model provides a good representation of different mechanisms influencing each other during and after the injection phase. Each mechanism affects the induced seismicity in a different way and at different times during the reservoir stimulation, confirming that a complex interaction is in place, and that more sophisticated and physics-based approaches coupled with statistical model are required to explain such a complex interaction. In addition to previous statistical and hybrid models, our approach accounts for a full 3D formulation of both stresses and fluid flow, further including all the TOUGH2 capabilities. Furthermore, it includes interactions between triggered seismic events through calculation of static stress transfer. In this work, we present the main capabilities of TOUGH2-SEED and apply the model to the Basel EGS case, successfully reproducing the injection pressure as well as the evolution of the seismicity.

1. Introduction

The exploitation of natural underground resources may raise concerns to the population for the risk of inducing earthquakes. Recently, it has been shown that anthropogenic activities, such as injection or withdrawal of fluids at depth, may cause induced seismicity. For example the seismicity rate has drastically increased in the United States midcontinent with earthquakes of magnitude 5 or more, within regions of active unconventional underground energy exploitation, and where the natural seismicity prior to the beginning

of the intense exploitation was rare or absent (e.g. Kerr, 2012; Keranen et al., 2014; Ellsworth et al., 2015). The potential hazard and risk for the affected population represents one of the main obstacles to the production of energy from deep underground resources, such as Enhanced Geothermal System, deep hydrothermal projects, and gas storage. Hence, studying how to prevent or reduce large induced earthquakes plays a pivotal role in the development and exploitation of future, innovative, and viable forms of natural deep underground resources.

The correlation between underground fluid injection and seismicity is an issue that has been extensively studied (e.g., Shapiro and Dinske, 2009; Ellsworth, 2013). With respect to natural seismicity, it is hard to discriminate between the relative contributions of induced fluid pressure and tectonic stress, but there are plenty of examples in the literature relating anthropogenic activity to local seismic events. Recently, a relative large number of reviews have been published (e.g report of the Committee on Induced Seismicity Potential in Energy Technologies of National Academy of Sciences – Hitzman et al., 2013). In more details, reviews have focused on: hydrocarbon fields (e.g. Suckale, 2009), deep high volume waste water related seismicity (e.g. Ellsworth, 2013; Frohlich et al., 2011), induced seismicityrelated to geothermal projects and other types of induced seismic events in Central Europe (Evans et al., 2012; Grünthal, 2014), hydraulic fracturing activities in relation to other activities (Davies et al., 2013), and CO_2 related gas storage activities (Nicol et al., 2011).

Exploitation of the natural underground resources requires the injection (or withdrawal) of fluid at depth. An open question is whether we can enhance fluid circulation in a safe way (e.g. aseismic or with low magnitude seismicity), by either stimulating a pre-existing fracture network or creating a new one. However, such circulation may also be increased along fault zones, which may result as a pathway for fluid to migrate upwards and possibly contaminate groundwater resources. Such an effect should be avoided if the injection is performed to store a gas (e.g. CO_2). Nowadays, no felt seismic events were associated to CO_2 storage around the world, despite several studies showing that the overpressure associated with the CO_2 injection can potentially induce seismicity (e.g. Mazzoldi et al., 2012),

reactivates large fracture at depth (Rinaldi and Rutqvist, 2013), and eventually results in leakage at shallow depth (Rinaldi et al., 2014a, Rinaldi et al., 2014b).

One problem of induced seismicity partially defies the current state of the art in modeling and risk assessment concepts, because: (a) the Earth crust is critically stressed in most places and crisscrossed with faults, but we rarely know the location of these faults and we do not have knowledge of their current state of loading; (b) the stress distribution and material properties at the scale of the reservoir are highly heterogeneous and also largely unknown.

During fluid injection, although seismicity is generally controlled by fluid overpressure (e.g., Rinaldi et al., 2014a, Rinaldi et al., 2014b, Rinaldi et al., 2015b), it is not possible to rule out some other mechanisms, such as static stress transfers between neighboring asperities, or temperature effects (Catalli et al., 2013, Catalli et al., 2016, Dublanchet et al., 2013). In these conditions, the relationship between fluid pressure and induced seismicity is much more complex. Moreover, while current modeling approaches focus mostly on the active injection phase, the static stress transfer may become important at later stages during the post-injection phase (Catalli et al., 2013, Catalli et al., 2016).

Many efforts in the last years aimed at a full understanding of coupled fluid flow and geomechanics processes, as well as induced seismicity. Studies have been performed accounting for lab experiments (e.g., Samuelson and Spiers, 2012; Guglielmi et al., 2015) as well as numerical modeling. The latter include: (a) fully coupled thermo-hydro-mechanical 3D numerical models (e.g., Rutqvist, 2011; Kolditz et al., 2012; Jha and Juanes, 2014; Rinaldi et al., 2015a), (b) purely statistical models (Bachmann et al., 2011, Shapiro et al., 2010), and (c) hybrid models combining statistical and physical considerations (e.g., Bachmann et al., 2012; Goertz-Allmann and Wiemer, 2013; Gischig and Wiemer, 2013; Gischig et al., 2014; Kiraly et al., 2014; Karvounis and Wiemer, 2015).

In the context hybrid models, we follow the so-called “seed model” proposed by Gischig and Wiemer (2013), of which we present here an improved version of the modeling approach. The transient pressure from TOUGH2 (Pruess et al., 2011) is used to calculate the stress changes on distributed “seed points”, representing potential earthquake hypocenters. Assuming a Mohr–Coulomb failure criterion, we evaluate at each time step if a seed point has the critical condition for reactivation given the pressure and temperature change at the seed location.

Employing TOUGH2 as the fluid flow simulator represents an improvement with respect to previous models (Gischig and Wiemer, 2013, Gischig et al., 2014), and it allows for a full 3D formulation. We also account for transient, implicit permeability changes, which depend on pressure variation. Moreover, we take into account the possibility of irreversible changes in permeability (e.g., due to hydroshearing): if a seed is reactivated, we calculate a further permeability enhancement (either slip- or plastic strain-dependent), which is then fed back to TOUGH2. We additionally improve the geomechanical-statistical model by accounting for 3D stress field and by including the orientation (dip and strike) for each possible earthquake location (seed). Furthermore, the TOUGH2-SEED model can also account for static stress transfer, allowing the reactivation of cascade events at the same time step, following approaches present in literature (e.g. Baisch et al., 2010; Catalli et al., 2016).

In this work, we first demonstrate the main capabilities of TOUGH2-SEED, presenting some base-case results. Then, we apply the model to simulate the injection at the EGS of Basel, Switzerland (Häring et al., 2008). For this test case, the model parameters are calibrated against observations of the injection-induced seismic sequence (i.e., wellhead pressure and rate of seismicity).

2. Modeling approach

2.1. Improvements to previous approaches

The proposed model closely follows the one introduced by Gischig and Wiemer (2013). However, in our updated version we use (i) TOUGH2 as fluid flow model, (ii) we update and improved the geomechanical-stochastic part

of the code to account for a realistic 3D state of stress, and (iii) we include the static stress transfer. The working scheme of our model is represented in detail by Fig. 1. We follow an explicit coupling scheme with TOUGH2 as main code. At each time step the TOUGH2 simulator computes fluid flow through the porous medium, and pore pressure (p) is passed to the SEED model, which is called internally by the main code.

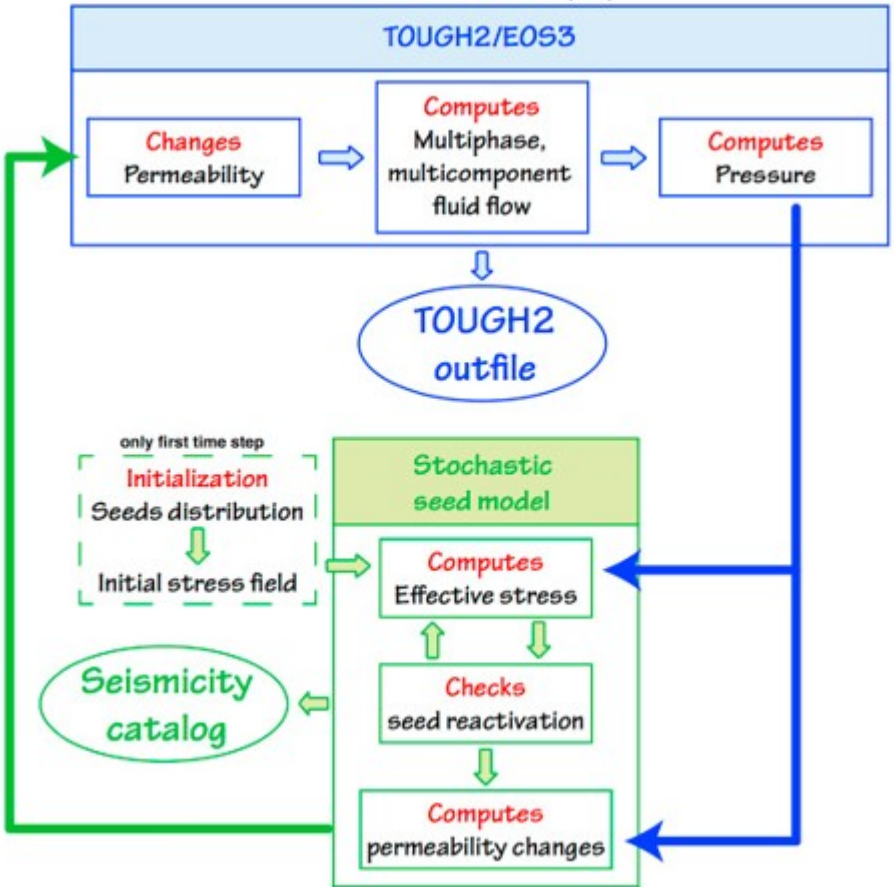

Fig. 1. Coupling scheme between TOUGH2 and the stochastic-mechanics seed model.

At first time step the SEED model distributes the seeds in the domain (random uniform or distributed on preferential structure), and computes the initial stress tensor for each seed based on user input (e.g. regional stress, number of seeds, etc.) and stochastic variation. While in Gischig and Wiemer (2013) the stress regime is defined by the two principal stress components, in our improved version we account for a 3D stress tensor at each seed location. The regional stress can be set as both strike-slip and dip-slip regime, with the possibility of orienting the stress in any direction. The initial three principal stress components of each seed are proportional to the

lithostatic, depth-dependent pressure (p_{lit}), plus a perceptual random variation to mimic heterogeneities in the stress field. The seeds represent potential earthquake hypocenters (i.e. point element). For each seed we define a theoretical plane (i.e. representing the fracture or the fault), and such a plane has a given orientation defined by a strike (φ) and dip angle (θ). While such planes are not explicitly simulated in the model, they are needed to compute stress conditions at the seed point.
After assigning initial conditions and at each time step, the pressure from TOUGH2 is interpolated at every seed location, and the diagonal terms of the effective stress tensor (σ_{ij}') of each seed are updated by the SEED model according to

$$\sigma'_{ij} = \sigma_{ij} - p\delta_{ij} \quad (1)$$

The current approach accounts for changes in effective stress due to pressure and/or transfer mechanisms (see below). However, no poroelastic deformation is computed.

The stress tensor is projected on the seed oriented plane, allowing computation of the shear τ and normal stress σ_n component. As described in detail by Zoback (2010), the principal stress tensor is projected first into geographical coordinates given the principal stress orientation; then, a further rotation is performed to compute the stress on the given plane with the slip orientation (rake, λ) given by the maximum shear stress.

At each time step the variations are computed at every seed location. Finally, following a Mohr-Coulomb criterion, seeds are reactivated if the shear stress (τ) is greater than the shear strength (τ_c), which is defined as $\tau_c = C + \mu\sigma_n$. Friction coefficient (μ) and cohesion (C) are assigned a priori with possible random deviation around an average value. The reactivation of a seed point is then associated to a seismic event, whose magnitude is randomly picked from a power-law distribution with a b-value corresponding to the seed differential stress (Goertz-Allmann and Wiemer, 2012; Scholz, 2015). Upon reactivation, the seed model also account for shear stress drop.

The stress drop, according to Gischig et al. (2014), is proportional to the normal stress and given by:

$$\Delta\tau = \Delta\tau_{coeff}\left(\frac{\tau - C}{\mu}\right) \quad (2)$$

where $\Delta\tau_{coeff}$ is an arbitrary coefficient and the shear stress is updated accordingly to $\tau_{new}=\tau-\Delta\tau$. If a stress transfer mechanism is activated (see below), the effective stress may change again, and the check for reactivation is iterated for every seismic event.

Finally, the SEED model calculates permeability changes due to pressure variation and/or seismicity for each gridblock. Such permeability changes are then fed back to TOUGH2 and are used to computes the fluid flow for the next time step. Such an explicit scheme has been proven to be successful for coupled simulations (e.g., TOUGH-FLAC; Rutqvist, 2011).

2.2. Static stress transfer mechanisms

An earthquake strongly alters the state of stress in the region surrounding the rupture plane. Such stress variation may affect other possible faults or fractures, bringing them closer to reactivation. Catalli et al. (2016) recently showed the importance of considering the stress interaction in an injection-induced seismic sequence, by retrospectively modeling the EGS stimulation at Basel. Their results demonstrate that the number of events is increased by the static stress transferring in comparison to a case where only the pore pressure is accounted as triggering mechanism.

In order to address such interaction between earthquakes, we include two possible models for static stress changes. The first one is the so-called “Spring-Block” model, firstly introduced by Baisch et al. (2010) and here generalized for a 3D formulation (Fig. 2a). Briefly, when a given seed is reactivated, the shear stress increases for neighboring seeds located within a volume *V*. We define such a volume as function of the rupture area, which represents the region where major slip and shear stress drop have occurred during the earthquake. Following empirical relationships (e.g., Wells and Coppersmith, 1994), such rupture area is defined as:

$$R_{eq} = \sqrt{\frac{7}{16}\frac{M_0}{\Delta\tau}} \quad (3)$$

where $\Delta\tau$ is the calculated stress drop, and $\log_{10}(M_0)=3/2\ M_w+9.1$, with M_w the moment magnitude. The stress changes may propagate further away from this rupture area, hence we assume the shear stress transferred within a volume $V=L^2\times W$, where $L=f_1\times R_{eq}$ and $W=f_2\times R_{eq}$, with f_1 and f_2 as input parameters. The amount of stress transferred within the volume is a fraction of the stress drop, with a larger stress being transferred along the slip direction (defined by the seed rake angle λ).

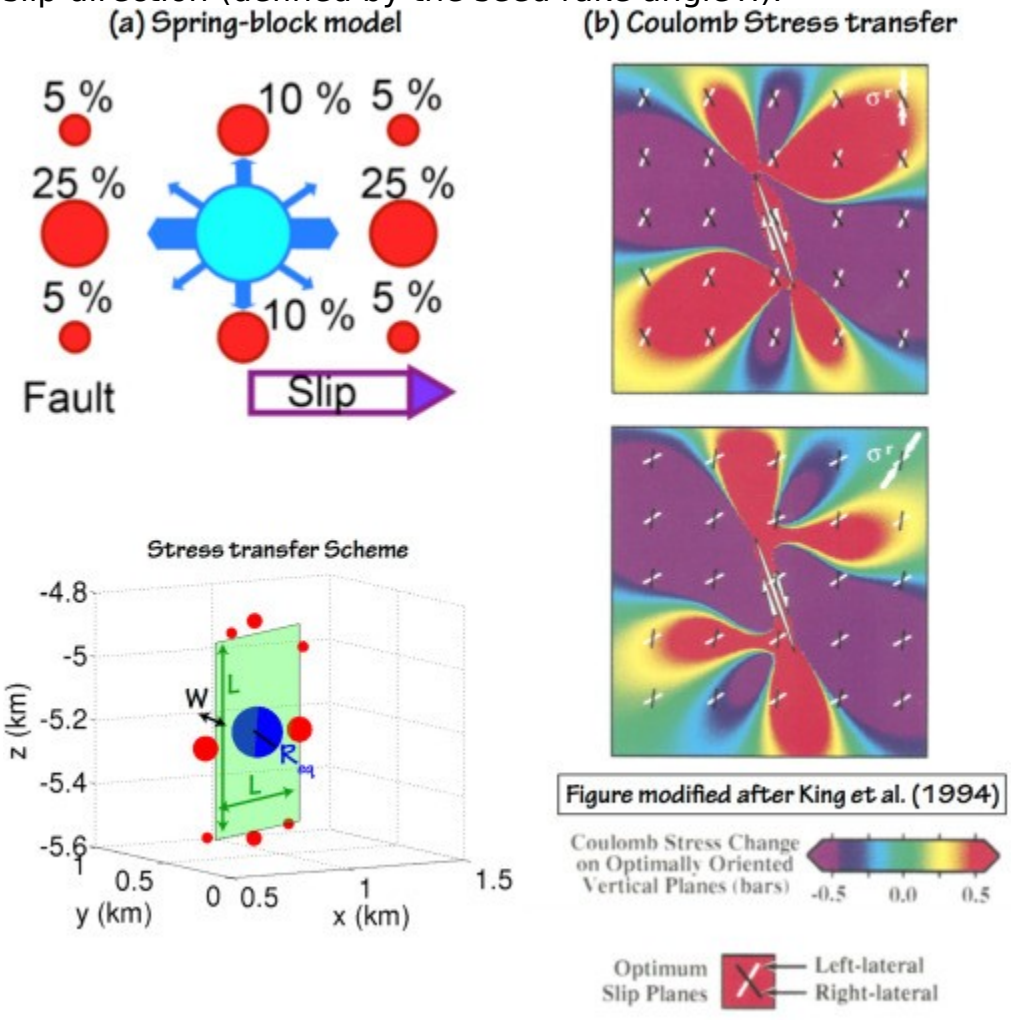

Fig. 2. (a) Upper figure: scheme for spring-block model as proposed by Baisch et al. (2010). Bottom: scheme of spring model as applied in this work. The stress drop associated to a given event is transferred according to above percentage to nearby seeds in a volume $L^2\times W$, as function of the

rupture area with $L=f_1 \times R_{eq}$ and $W=f_2 \times R_{eq}$, and f_1 and f_2 as input parameter. (b) Figure modified after King et al. (1994). The rupture on a given fault will produce variations in Coulomb stress. Such changes depends on the orientation of both source and receiver faults.

The second model considers static stress transfer as a classical Coulomb stress interaction, following the recent modeling effort by Catalli et al. (2016). The reactivated seed is modeled as a source of Coulomb stress (ΔCFS_{int}), which is then transferred to neighbor seeds. Dimension of the source and slip magnitude follow empirical relationship (Wells and Coppersmith, 1994), and each seed fault is considered as a rectangular source (Okada, 1992). An increase in Coulomb stress brings the seeds subjected to such a change closer to reactivation. Compared to the spring-block model, the Coulomb stress transfer also allows for the creation of stress shadow regions (i.e., negative stress changes), as described by King et al. (1994) and shown here in Fig. 2b for different orientation of the regional stress.

2.3. Permeability changes

Several approaches have been proposed to address the relationship between stress and hydromechanical properties. Rock permeability is often related to changes in fracture aperture, which is generally a function (exponential or inverse relationship) of the normal effective stress (Rutqvist, 2015). Permeability can also be related to fault reactivation through evaluation of plastic failure (e.g. Rinaldi et al., 2014a, Rinaldi et al., 2015a). Authors (e.g. Garg and Pritchett, 1984) have also shown that temperature effects on permeability can be important when injecting cold water into hot rock, especially for near-wellbore variations.

In TOUGH2-SEED, we account at this stage for two possible mechanisms for permeability changes: (i) pressure and/or (ii) slip on a given seed.

The first mechanism is a reversible pressure-dependent permeability relationship (updated after Rinaldi et al., 2014a):

$$\kappa_{hm} = \kappa_0 e^{C_1\left(\frac{\phi_{hm}}{\phi_0}-1\right)}, \quad \phi_{hm} = \left(\phi_0 - \phi_r\right) e^{\varsigma \Delta p} + \phi_r \tag{4}$$

where $C_1$and ς are two empirical coefficients that are set as input parameters. The permeability at the current state of pressure (κ_{hm}) is function of the current porosity (ϕ_{hm}), which directly depends upon the pressure changes (Δp). ϕ_0 and ϕ_r are initial stress-free porosity and the residual porosity, respectively. κ_0 is the initial permeability. This mechanism allows for a smooth permeability variation, hence accounting for pores and fractures to be elastically opened. At this stage, the porosity changes (ϕ_{hm}) are only computed to evaluate their effects on the permeability (κ_{hm}), but they are not fed back to TOUGH2, hence not contributing in mass or energy changes.

The second mechanism accounts for permeability variations due to the seismic events, and it is based on a slip-dependent equation (Gischig et al., 2014):

$$\kappa = \kappa_0 \left[1+C_2 \left(1-e^{\frac{-\Delta d}{d^*}}\right)\right]^n, \Delta d = \frac{M_0 \left(\frac{16\Delta\tau}{7M_0}\right)^{\frac{2}{3}}}{G\pi} \quad (5)$$

where C_2 is a constant coefficient, d^* represents the slip scale, G is the shear modulus, $\Delta\tau$ is the calculated stress drop, and $\log_{10}(M_0)=3/2\ M_w+9.1$, with M_w the moment magnitude. This mechanism represents a very localized permeability variation, close to the triggered seeds (e.g., fracture opening, or slip on a fault zone), although in our model the permeability change is assigned to the gridblock containing the reactivated seed. It is worth of note that this permeability depends on the seismic moment, hence on the magnitude, which is randomly assigned.

3. Base case applications

In the following section we demonstrate the potential of TOUGH2-SEED by simulating some basic, synthetic cases of injection-induced seismicity. The simulations are aimed at showing the effect of the two permeability change mechanisms on spatial and temporal distribution of the seismic cloud, as well as demonstrating the effects of stress interactions between the different seeds. We run 120 realizations for each base case setup, to account for the stochastic behavior of the proposed approach, and results are presented including one standard deviation error.

3.1. Model setup

The model domain for all the base case simulations is 4×4 km wide and 4 km deep (from −2 to −6 km depth), with a total of 20,425 elements. The mesh is finer in the central area of the domain, where we simulated a step-injection of cold water up to 10 days. The injection well is simulated as composed by a closed section with high vertical permeability, and an open section, which is directly connected to the main computational meshgrid (Fig. 3a). The fluid injection occurs at a depth of 4300 m, with a rate increasing from 5 kg/s up to 50 kg/s (Fig. 3b). The shut-in occurs after 10 days of continuous injection. The choice of 10 days injection is in agreement with the length of a single stimulation step and it has similar duration as observed at several sites (e.g., 6 days at Basel – Häring et al., 2008; 12 days at Soultz – Evans et al., 2005; 15 days at Newberry – Cladouhos et al., 2015), although for some EGS the stimulation may occur over a longer period (e.g., 250 days at The Geysers – Jeanne et al., 2015). All the boundaries are open with fixed hydrostatic and geothermic conditions. The initial permeability is uniform over the entire domain corresponding to 10^{-16} m^2, with 1% porosity. Initial hydraulic conditions include hydrostatic pore pressure and linear temperature gradient. Initial stresses on the seeds are assigned following a strike slip regime, with average proportion to the lithostatic stress ($\sigma_H = 1.3\sigma_V$, $\sigma_h = 0.7\sigma_V$) and with 10% random variation around the mean value. The maximum horizontal stress is oriented along the *x*-axis (or *EW*-direction), with the *z*-axis representing the vertical direction.

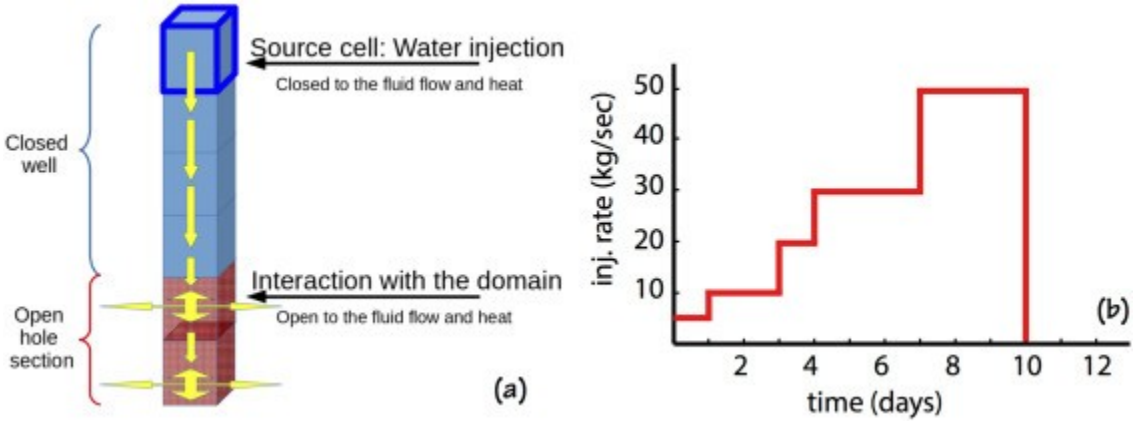

Fig. 3. (a) Approach for modeling injection well, simulated as composed by a closed and an open section, which is the only portion of the well connected to the main TOUGH2 mesh. Yellow arrows indicate the possible flow direction. (b) Injection rate for the base case simulations.

We spatially distribute 35,000 seeds, with the majority of the seeds (25,000) uniformly distributed in a region 2×2×2 km around the injection well. This assumption does not necessarily represent a real case, in which we could assume different densities of seeds in different zones of the domain, according to the observed seismicity of the area. We enable such a feature in the code by accounting for the possibility of distributing the seeds on a preferential region as shown in one example case below. We assign an average value of 0.6 for the frictional coefficient, with a possible random variation of 0.05. All the seeds are assumed to be optimally oriented with fixed strike angle of 60° and dipping 90°. Although the code is constructed to account for variation in seeds orientation (i.e., strike and dip), for simplicity, we assume a fixed orientation of the seeds for most of the base cases, unless specified in the text. Table 1 reports all the constant parameters used in the simulations.

Table 1. List of constant parameters used in the base case simulations.

Thermal expansion (β)	$3 \cdot 10^{-5}$ °C^{-1}
Shear modulus (G)	10 GPa
Poisson ratio (ν)	0.25
Rock density (ρ)	2500 kg/m^3
Initial porosity (ϕ_0)	1%
Residual porosity (ϕ_r)	0.5%
Initial permeability (κ_0)	10^{-16} m^2
Porosity-equation constant – C_1	15
Pressure-equation exponent – α	10^{-8} Pa^{-1}
Slip-equation constant – C_2	2
Critical slip (d^*)	$2 \cdot 10^{-3}$ m
Cohesion (C)	2 MPa
Stress drop coeff. ($\Delta\tau_{coeff}$)	0.05
Min-Max magnitude	0.9–9
Min-max differential stress	

for *b*-value	0–136 MPa
f_1 for Spring-Block	3
f_2 for Spring-Block	0.25

3.2. Comparison of permeability changes

The first set of simulations aims at showing the response of the system in terms of seismicity when accounting for an irreversible variation in permeability. While the first simulation (referred as Simulation 1) only accounts for reversible pressure-dependent permeability changes (Eq. (4)), the second case (Simulation 2) accounts for slip-dependent permeability in addition to the reversible variation (Eq. (5)). In both cases, we do not account for the stress transfer at this stage.

Fig. 4 shows the temporal response for the wellhead pressure and for the rate of seismicity for both cases. In the case of reversible permeability changes (Simulation 1), we obtain a rate of events up to 60 events per 12 h, with a stochastic variation of up to 10 events/12 h (Fig. 4a). In terms of wellhead pressure, we obtain up to a variation of 40 MPa when injecting at 50 kg/s (Fig. 4a, blue line). In this case, the seed model does not interact with TOUGH2, hence no stochastic variation is observed in the pressure evolution. In Simulation 2, which accounts for irreversible changes in permeability as related to the seismic events, the evolution of the pressure is quite different. We observe a lower pressure increase (up to 25 MPa as average variation) and a quite strong stochastic variation, with up to 10 MPa for 1 standard deviation for the 120 realizations (Fig. 4b, blue line and area). The evolution of seismicity is similar to the first case and with a similar stochastic variation, although with a lower rate given the average low pressure (up to 50 events per 12 h – Fig. 4b, red line and area). Generally, accounting for slip-dependent permeability means that the permeability presents a larger and faster variation when a large number of events occur. Such variation may result in spiked-like pressure changes, although not visible when averaging over 120 realizations.

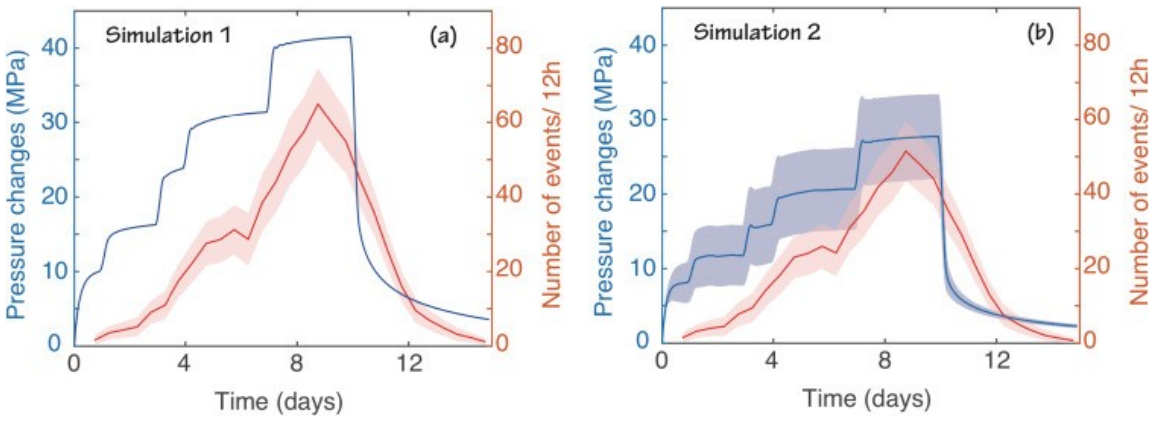

Fig. 4. (a) Simulation 1: Bottomhole pressure (blue line) and average simulated number of events for every 12 h with standard deviation (red line and area, respectively) for the case of permeability only depending on pressure. (b) Simulation 2: Average bottomhole pressure (blue line) and simulated number of events for every 12 h (red line) for the case of permeability depending on both pressure and event slip. Both variables here are presented with 1 standard deviation area (blue and red area for pressure and number of events, respectively). The average and standard deviation are calculated over 120 realizations.

Fig. 5 shows the horizontal distribution of pressure and seismicity at 7 and 10 days of stimulation for a single realization for both Simulation 1 and Simulation 2 at depth of injection. The pressure variation in Simulation 1 reaches a maximum around injection zone of about 25 MPa (Figs. 5a and b), while in Simulation 2 the pore pressure variations are lower given larger permeability changes: around 10 MPa at 7 days, and not exceeding 15 MPa after 10 days of stimulation (Figs. 5c and d). In terms of seismicity, the events are generally confined within the region of pore pressure changes. For both cases, events occur in a box of 1 km^2 around the injection point at 7 days (Figs. 5a and c), and the seismic cloud only extends a few hundreds meters more after 10 days of stimulation (Figs. 5b and d). A larger number of events occur for Simulation 1 nearby the injection well, caused by retriggering of previously reactivated faults given the larger pressure (~25 MPa). Such larger number of events nearby the injection well explains the higher rate of seismicity (Fig. 4a) with respect to Simulation 2, although the extent of the seismic cloud is similar for the two cases.

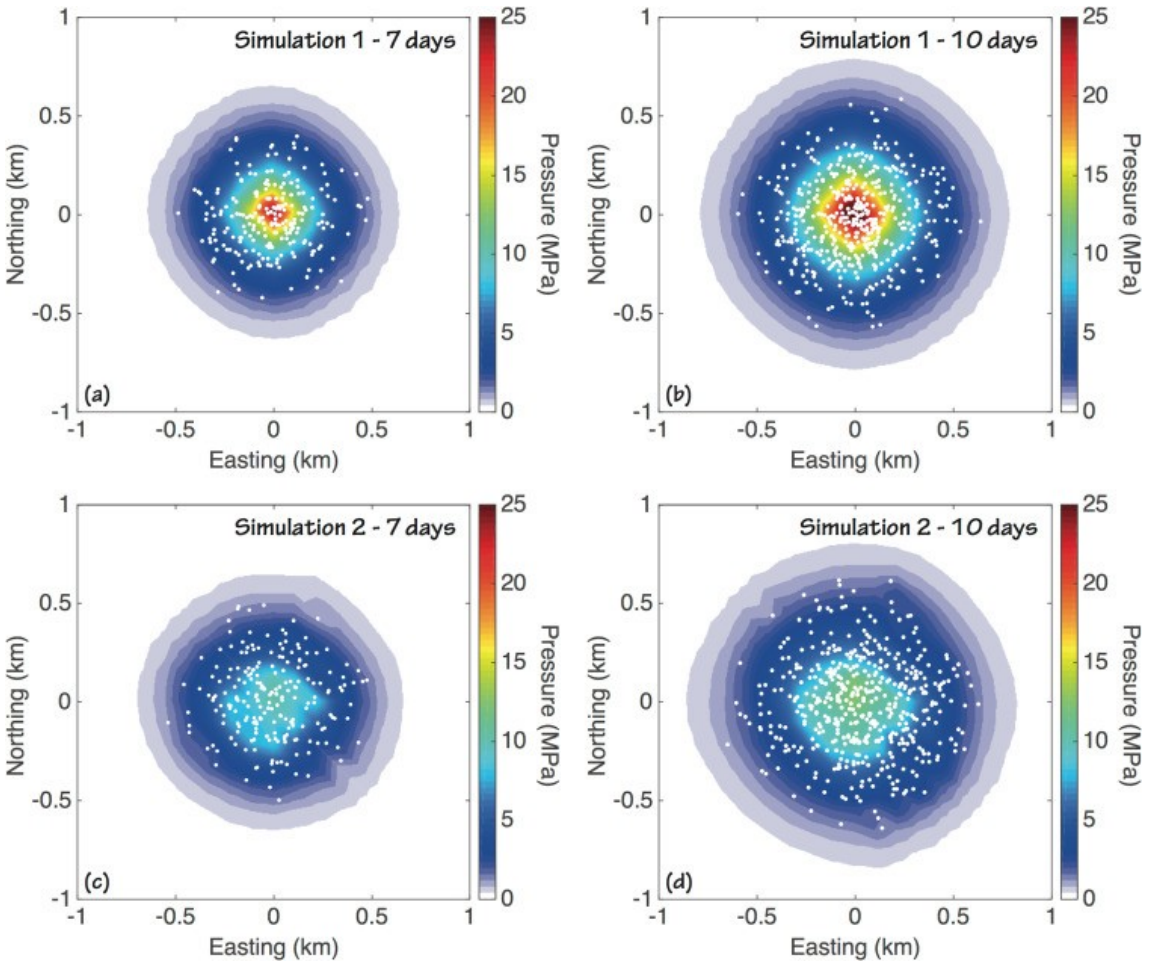

Fig. 5. Pressure distribution (contour) and events location (white dots) at 7 (a) and 10 (b) days for the case of permeability only depending on pressure (Simulation 1), at 7 (c) and 10 (d) days for the case of permeability depending on both pressure and slip (Simulation 2). The results are for a single realization.

Fig. 6 shows the horizontal and vertical sections of permeability in the two simulations at the end of the injection period for a single realization. Simulation 1 shows permeability changes up to an increase of one order of magnitude (up to 10^{-15} m^2) nearby the injection zone (Figs. 6a and b). Given Eq. (4), the permeability evolution strictly follows the pore pressure distribution. In Simulation 2, the effects of the two mechanisms of permeability enhancement are overlapped (Figs. 6b and d). Indeed, given Eq. (5), a triggered seed produces a localized permeability increase, whose magnitude depends on the stress drop and seismic moment, which is randomly assigned for each event. In Simulation 2, this relation between permeability and slip leads to scattered permeability changes up to

10^{-14} m^2 (i.e., a two orders-of-magnitude increase). Worth of note is that the chosen permeability dependency may lead to a different shape of overpressure in the domain: while in Simulation 1 the injection-induced overpressure evolves along an almost spherical front, in Simulation 2 the evolution is slightly anisotropic, especially along the vertical direction for the considered realization (Fig. 6d).

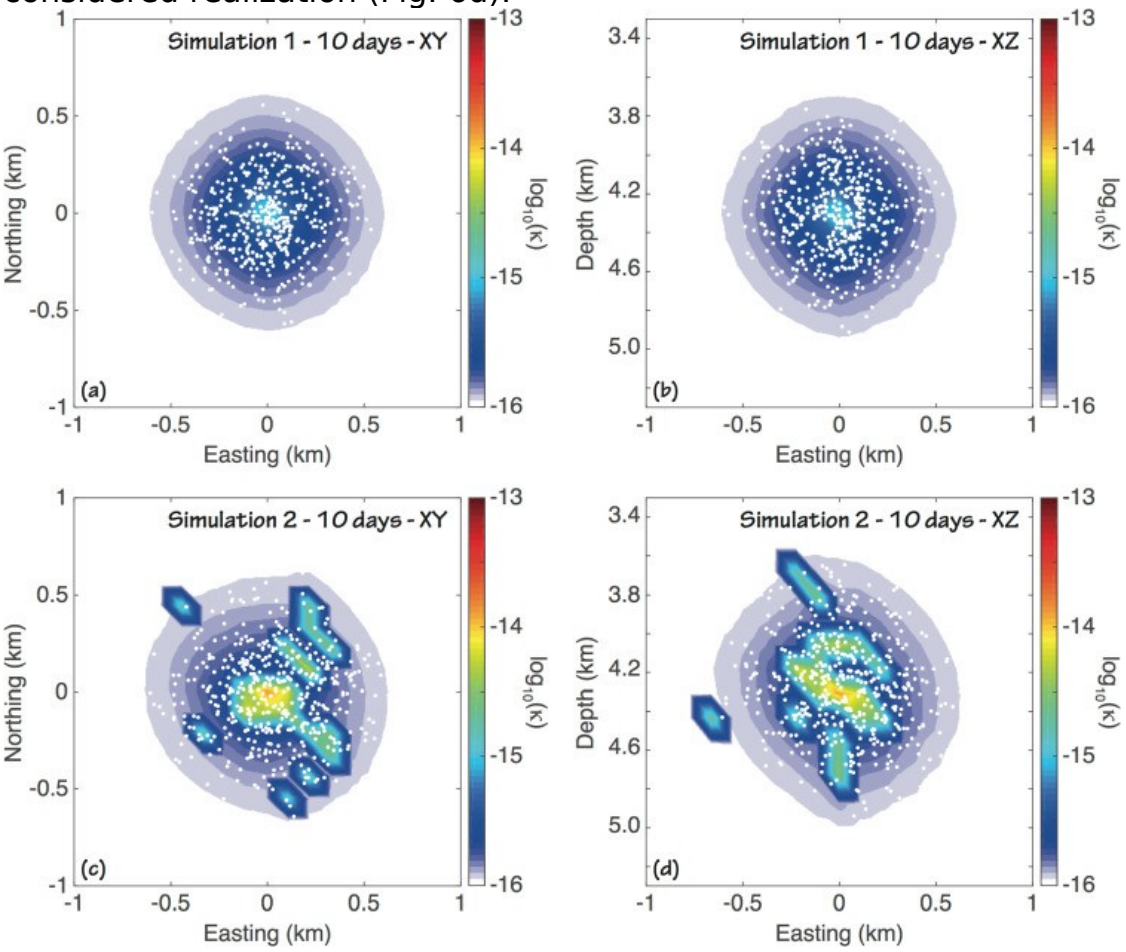

Fig. 6. Permeability (logarithm, contour) and events location (white dots) after 10 days for *XY* (a) and *XZ*(b) planes for the case of permeability only depending on pressure (Simulation 1), after 10 days for *XY* (c) and *XZ* (d) planes for the case of permeability depending on both pressure and slip (Simulation 2). The results are for a single realization.

3.3. Stress transfer

Recent works highlight the importance of considering earthquake interaction during an injection-induced sequence (Catalli et al., 2013, Catalli et al., 2016). The static stress transfer may increase the observed number of

events, particularly when the seismicity is occurring over a preferential structure (Schoenball et al., 2012, Catalli et al., 2016).

As a further base case applications of TOUGH2-SEED, we performed two more simulation cases aimed at showing the effect of static stress transfer on a seismic sequence caused by fluid injection. We simulate two additional setups by using the Coulomb and the Spring-Block models, respectively. In both cases permeability can change irreversibly as function of both pressure and slip.

Fig. 7a shows the comparison between the two static stress transfer models and the base case of no earthquake interaction, as averaged over 120 realizations. We observed that a larger cumulative number of events is triggered at the end of simulation when considering the stress transferring compared to the case of no interaction. The number of events increases by about 12% and 29% for the Coulomb and Spring-Block model, respectively, compared to the case of no interaction. The difference between the three models further increases if the seeds are mainly distributed along some preferential direction. Assuming a large density of seeds in a box 100 m wide, oriented with strike 60° and dip 90°, the number of events increases compared to the case of no interaction by about 28% and 70% for Coulomb and Spring-Block model, respectively, although the latter with about 20% standard variation (Fig. 7b). Worth noting that the Spring-Block does not consider for stress shadow and strongly increases the seismicity for seeds aligned on a plane, depending on the factors for defining the volume of interaction ($L^2 \times W$, with $L = f_1 \times R_{eq}$ and $W = f_2 \times R_{eq}$).

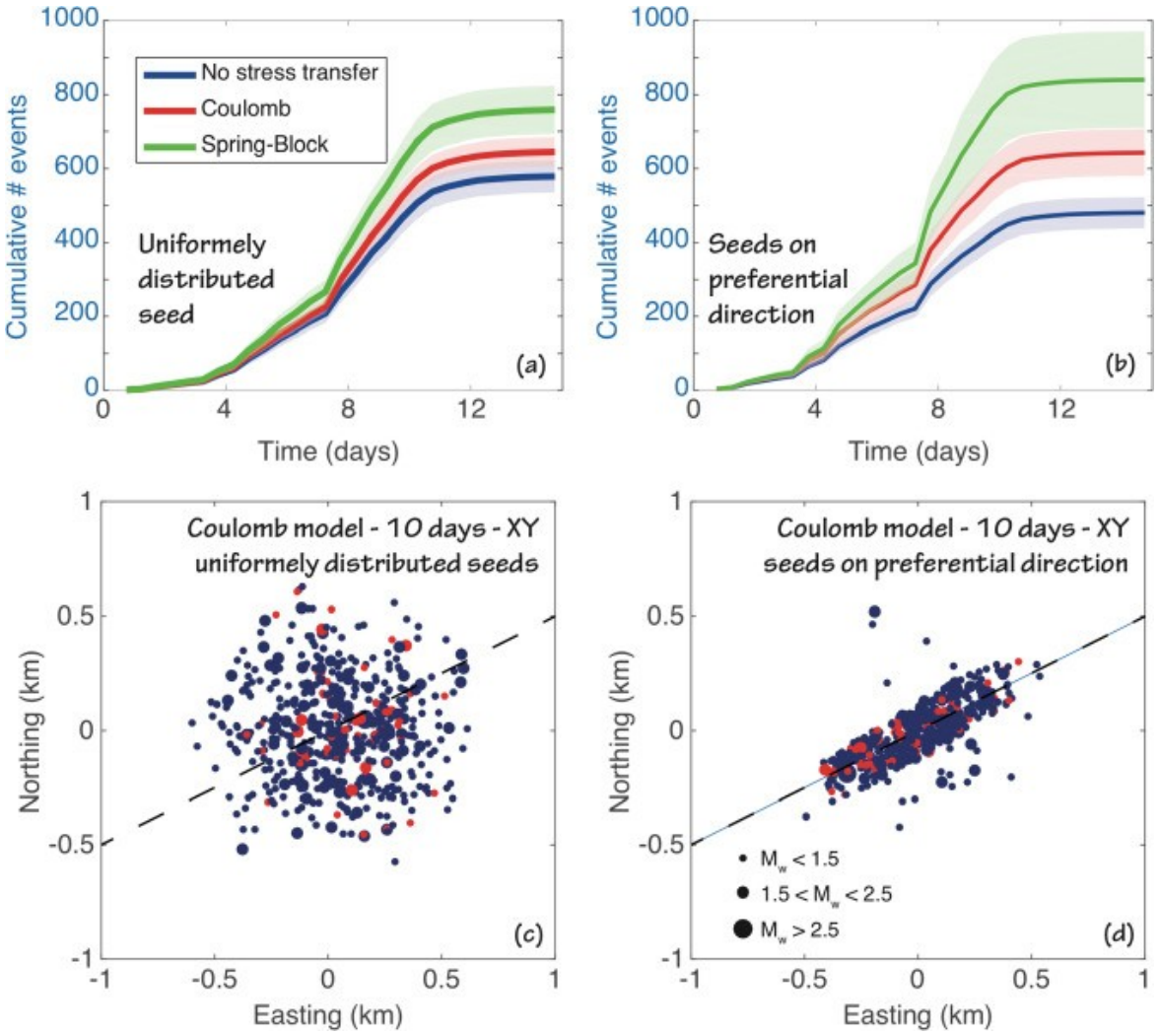

Fig. 7. (a) Cumulative number of events average over 120 realization for the cases of no stress transfer (blue), Coulomb model (red), and Spring-Block model (green), for a uniform random distribution of seeds. (b) Cumulative number of events average over 120 realization for the cases of no stress transfer (blue), Coulomb model (red), and Spring-Block model (green), for a distribution of seed on a preferential region (e.g. a fault zone). Such a region for these realizations is 2×2×0.1 km^3 with 60° strike orientation. The shaded areas in panel (a) and (b) represent the standard deviation for the respective model. (*c*-d) Example distribution of seismicity at depth of injection for a single realization accounting for Coulomb stress transfer for the cases of uniform and preferential distribution, respectively. The red dots represent the events primarily triggered by stress transfer.

As already highlighted by Catalli et al. (2016), the stress transfer is more effective in the stimulated region. Our results further justify the previous findings, as shown in Fig. 7c for a single realization considering Coulomb stress interaction. Red dots in both figures represent the events primarily

triggered by stress transfer, although both pressure and stress transfer act in synergy to bring the seed to failure and it is not trivial to separate the two contributions. Fig. 7d shows an example of triggered seeds for a single realization with preferential distribution. Most of the seeds are triggered along the preferential plane, although some events still occur off-plane.

4. Real case application

4.1. The basel enhanced geothermal system

The case of Basel (Switzerland) is widely studied because of the large number of data and measurements obtained during and after a partial stimulation of an Enhanced Geothermal System (EGS). The “Basel case” is very useful to study the relationship between deep fluids injection and induced seismicity, and it can be suitably used as a benchmark to test the potential of TOUGH2-SEED.

At Basel EGS, the stimulation started on December 2nd, 2006 and lasted for 6 days until the M_L=2.6 earthquake that happened on December 8th (Häring et al., 2008). Theoretically the injection phase was planned to last 21 days, but due to the high seismicity rate, the injection was initially reduced and finally stopped, only to start bleeding-off the well after the occurrence of a M_L=3.4 (Fig. 8a).

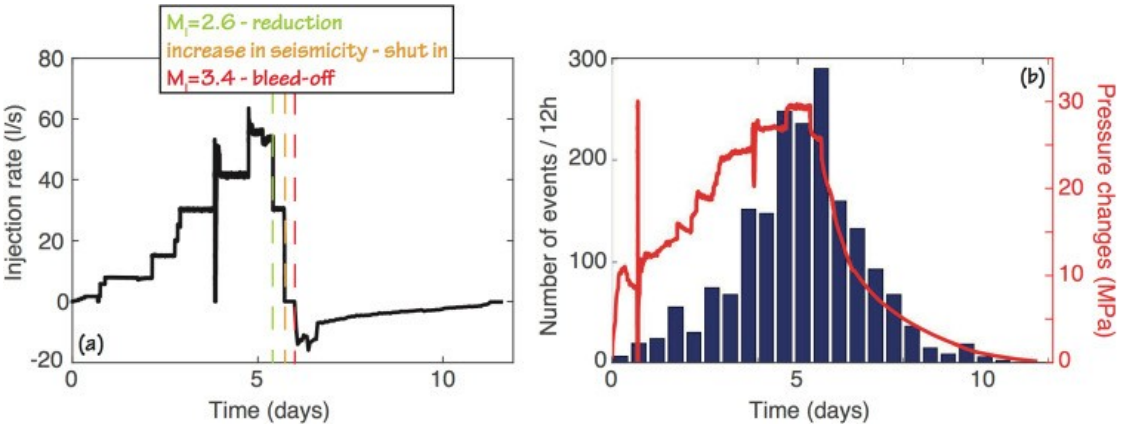

Fig. 8. (a) Injection rate during the stimulation of the Basel EGS. (b) Wellhead pressure (red) and rate of events per 12 h (histogram). Catalog from Bachmann et al. (2011), with a magnitude of completeness M_c=0.85.

During the stimulation about 11,000 m^3 of water were injected and more than 10,000 earthquakes were induced around the injection well at about −4.5 km depth (Häring et al., 2008, Catalli et al., 2013). The injection rate was increased in steps up to a maximum of 63 l/s, with the wellhead pressure evolution generally following the injection rate trend reaching its maximum (29.6 MPa) at the end of the stimulation (Fig. 8b). The two spikes of the wellhead pressure are related to mechanical repairs of the well. The seismicity blandly followed the injection rate evolution (Fig. 8b): the number of events increased progressively during the injection phase and rapidly decreased after shut-in, although three other events of magnitude greater than M_L=3 occurred within the following 2 months (Bachmann et al., 2011). The seismicity is mainly distributed in a nearly vertical plane centered at −4.5 km of depth with an azimuth of 155°. Such orientation is in accordance with the regional stress field, which characterized by strike-slip regime with the maximum horizontal stress orientated along NW direction (Häring et al., 2008 and references therein). The maximum horizontal stress was estimated at a value between 160 and 255 MPa, while minimum principal stress and vertical stress were estimated at 84 MPa and 122 MPa, respectively (Häring et al., 2008). Measurements of the principal stress components orientation were performed by Valley and Evans (2009), which found a mean orientation of maximum horizontal stress of 144±14° and a minimum horizontal stress of 54±14°.

4.2. Modeling setup

The modeling domain and initial hydraulic conditions are the same as employed for the base case simulations. The material is homogeneous over the entire domain with an initial permeability of $1 \cdot 10^{-17}$ m^2 and a porosity of 0.5% (Häring et al., 2008). The injection rate evolution is same as in the Basel stimulation (Fig. 8a). 5000 seeds are distributed over the vertical domain, with a larger density in a vertical square box 3×3 km^2, with a width of 100 m. Such a box is oriented with the same strike as the seismicity cloud observed at Basel (155°). A further 1600 seeds are randomly distributed over the entire domain. This distribution takes into account the anisotropy of the geological setting due to presence of natural fractures mainly oriented NW-SE and NNW-SSE (Häring et al., 2008). Such natural fractures can foster the propagation of the seismic activity along a preferential direction. Each seed

represents a fault with strike oriented along the high-density seed distribution direction and a dip=90°, with a normal variation of 15° around the average value (Catalli et al., 2016). A complete list of model parameters is listed in Table 2. Such parameters reflect a good choice for fitting the data, although no residual analysis was performed at this time. We performed 120 realizations to account for stochastic variation of seeds coordinates, stresses magnitude and orientation, and frictional coefficient.

Table 2. List of constant parameters used in the Basel EGS case.

Thermal expansion (β)	$3 \cdot 10^{-5}$ °C^{-1}
Shear modulus (G)	5 GPa
Poisson ratio (ν)	0.25
Rock density (ρ)	2500 kg/m^3
Initial porosity (ϕ_0)	0.5%
Residual porosity (ϕ_r)	0.1%
Initial permeability (κ_0)	10^{-17} m^2
Porosity-equation constant – C_1	15
Pressure-equation exponent – α	10^{-8} Pa^{-1}
Slip-equation constant – C_2	1.42
Critical slip (d^*)	$2 \cdot 10^{-3}$ m
Cohesion (C)	3 MPa
Stress drop coeff. ($\Delta\tau_{coeff}$)	0.06
Min-Max magnitude	0.85–9
Min-max	

differential stress for *b*-value	0–136 MPa
σ_H (at 5 km depth)	196 MPa±2% (160–255 MPa inHäring et al., 2008) orientation: 144±14° (Valley and Evans, 2009)
σ_V (at 5 km depth)	123 MPa±2% (~122 MPa inHäring et al., 2008) orientation: vertical
σ_h (at 5 km depth)	75 MPa±2% (~84 MPa inHäring et al., 2008) orientation: 54±14° (Valley and Evans, 2009)

4.3. Modeling results

Fig. 9a shows the comparison between the simulated and the measured wellhead pressure evolutions. The set of simulations allows representing with good approximation the pressure evolution during the entire injection phase, within one standard deviation for the 120 realizations. The largest differences are observed after the shut-in phase (6 days) where the simulated pressure recovery is faster than the real evolution. This effect could be related to the wellbore model: after the shut-in and the bleed-off, the well remained open and produced a total back flow of about 3400 m^3 of water (Häring et al., 2008) that we are not simulating. Another possible cause for the mismatch is the lack of detailed near-wellbore permeability changes, which could be related to cooling due to cold-water injection as well as to mechanical stress changes occurring within the wellbore itself.

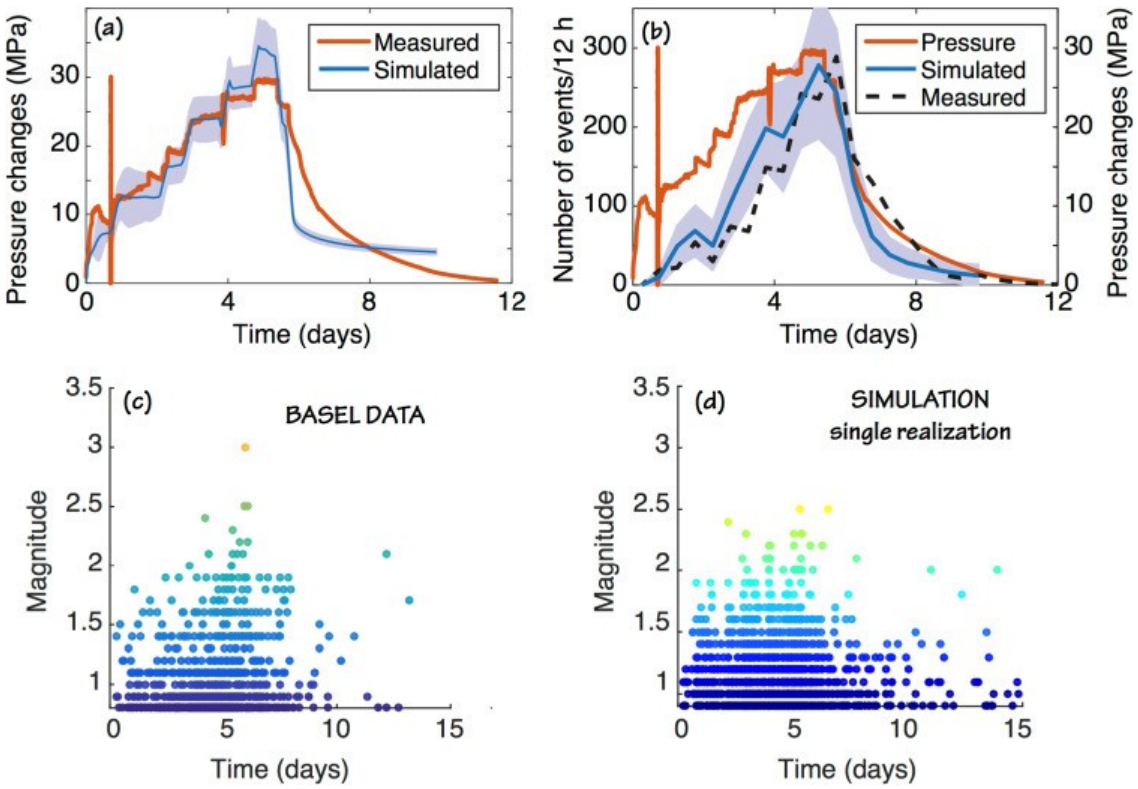

Fig. 9. (a) Comparison between the measured (red, dashed line) and the simulated (blue) wellheadpressure. The shaded blue area represents the standard deviation over 120 realizations. (b) Comparison between observed (blue, dashed line) and simulated rate of seismicity (red line). The shaded red area is the standard deviation over 120 realizations. Figure also includes the measured well pressure (green line) for reference. (*c*-d) Magnitude of events over time for Basel catalog (Bachmann et al., 2011 – with M_c=0.85) and one single realization results, respectively.

The model reproduces the total number and temporal distribution of seismic events (Fig. 9b). Simulation results (red line, with area representing one standard deviation) follow the overall increase during the whole injection phase, reaching a maximum number of 300 events per 12 h (around day 6) right after the reduction of flow. After the shut-in the number of events rapidly drops following the pressure curve. However, at the end of the simulations (15 days) few events are still triggered. In the post shut-in phase the pore pressure is lower and the static stress transfer can play a greater role in triggering induced seismicity after several days (Catalli et al., 2016). Figs. 9c and d plot the magnitude over time for the real and for one single model realization, respectively. The event magnitude occurrence over time is quite well represented by the model. The events with large

magnitude (M>2) are in both cases taking place between day 3 and 7, with the largest one after shut-in.

5. Conclusion

In this paper we presented some features of the code TOUGH2-SEED. Such a simulator couples the capabilities of TOUGH2 as fluid flow simulator to a geomechanical-stochastic code for the study of injection-induced seismicity during deep underground exploitation.

We presented some base case applications of the code. Simulation 1 and Simulation 2 showed the effects of two different permeability enhancement processes, over a statistically relevant number of realizations. Assuming a reversible pressure-dependent permeability we obtained a regular and well-defined seismicity zone around the injection well. Considering irreversible slip dependent permeability changes, we obtained a more scattered permeability evolution that can consequently influence the pore pressure evolutions and then the whole seismicity.

TOUGH2-SEED also accounts for stress transfer effects. The most trivial consequence of the stress transfer is that it brings the seed closer to failure, and it may lead to cascade events: the stress transfer not only influences the number of events, but also their spatial and temporal distribution. Results of base case applications further confirmed recent findings, and show that the stress interaction may largely increase the number of seismic events if feature clustering seismicity are presented in the field (e.g. fault zone).

Finally, we applied the code to model the well-studied case of Basel Enhanced Geothermal System. The application shows that a complex model, accounting for fluid flow, mechanical effects, and evolving hydraulic parameters, is better suited to properly reproduce most of the characteristic behavior. For the Basel case, TOUGH2-SEED represents a correct initial stress field, while satisfactorily reproducing the temporal events distribution and their magnitude.

We demonstrated that the TOUGH2-SEED model can simulate, up to a certain extent, the complex interaction of fluid flow and seismicity. Compared to previous models, we account for a more sophisticated fluid flow simulator, such as TOUGH2. Moreover, our improvements to the geomechanical-stochastic seed model allow capturing some effects that are impossible to represent on a simpler 2D model.

Although several effects are not considered (e.g., poroelasticity, fracture creation/propagation), the TOUGH2-SEED model constitutes a further step to the representation of physics-based processes in a statistical model. The mechanical coupling can influence the seismicity at very different spatial and temporal scales, leaving open the way for the creation of more complex and realistic models.

Acknowledgments

This work was mainly supported by a SNSF Ambizione Energy grant (PZENP2_160555) and partially financed by a research agreement between the Swiss Seismological Service (SED) and the Swiss Federal Nuclear Safety Inspectorate (ENSI). The work by Massimo Nespoli was carried out when the author was enrolled in the Doctorate school at the University of Bologna, on a grant funded by the Istituto Nazionale di Geofisica e Vulcanologia – Sezione di Bologna. Technical review comments by Dimitrios Karvounis and Eszter Kiraly at SED are all greatly appreciated. A. P. Rinaldi thanks Francesca Vitalini for editorial review.

References

1. Bachmann et al., 2011
C.E. Bachmann, S. Wiemer, J. Woessner, S. Hainzl **Statistical analysis of the induced Basel 2006 earthquake sequence: introducing a probability-based approach for Ehnhanced geothermal system** Geophys. J. Int., 186 (2011), pp. 793-807, 10.1111/j.1365-246X.2011.05068.x

2. Bachmann et al., 2012
C.E. Bachmann, S. Wiemer, B.P. Goertz-Allmann, J. Woessner **Influence of pore-pressure on the event-size distribution of induced earthquake** Geophys. Res. Lett., 40 (1) (2012), pp. 72-77, 10.1029/2012GL051480

3. Baisch et al., 2010
S. Baisch, R. Vörös, E. Rother, H. Stang, R. Jung, R. Schellschmidt **A numerical model for fluid injection induced seismicity at Soultz-sous-Forêts**
Int. J. Rock Mech. Min. Sc., 47 (3) (2010), pp. 405-413, 10.1016/j.ijrmms.2009.10.001

4. Catalli et al., 2013
F. Catalli, M.-A. Meier, S. Wiemer **The role of coulomb stress changes for injection-induced seismicity: the Basel enhanced geothermal system**
Geophys. Res. Lett., 40 (1) (2013), pp. 72-77, 10.1029/2012GL054147

5. Catalli et al., 2016
F. Catalli, A.P. Rinaldi, V. Gischig, M. Nespoli, S. Wiemer **The importance of earthquake interactions for injection-induced seismicity: retrospective modeling of the Basel enahnced geothermal system**
Geophys. Res. Lett. (2016), 10.1002/2016GL068932

6. Cladouhos et al.,
Cladouhos, T.T., Swyer, M.W., Uddenberg, M., and Petty, S., 2015. Results from Newberry volcano EGS demonstration, In: Proceedings of the 40th Workshop on Geothermal Reservoir Engineering, Stanford University, Stanford, California, USA, February 26-28, SGP-TR-204.

7. Davies et al., 2013
R. Davies, G. Foulger, A. Bindley, P. Styles **Induced seismicity and hydraulic fracturing for the recovery of hydrocarbons**
Mar. Petrol. Geol., 45 (2013), pp. 171-185, 10.1016/j.marpetgeo.2013.03.016

8. Dublanchet et al., 2013
P. Dublanchet, P. Bernard, P. Favreau **Interactions and triggering in a 3-D rate-and-state asperity model**
J. Geophys. Res. – Solid Earth, 118 (5) (2013), pp. 2225-2245, 10.1002/jgrb.50187

9. Ellsworth, 2013
Ellsworth **Injection-Induced earthquakes**
Science, 341 (6142) (2013), 10.1126/science.1225942

10. Ellsworth et al., 2015
W.L. Ellsworth, A.L. Llenos, A.F. McGarr, A.J. Michael, J.L. Rubinstein, C.S. Mueller, M.D.Petersen, E. Calais **Increasing seismicity in the U. S. midcontinent: implications for earthquake hazard**
Lead. Edge, 34 (6) (2015), pp. 618-620, 10.1190/tle34060618.1

11. Evans et al., 2012
K.F. Evans, A. Zappone, T. Kraft, N. Deichmann, F. Moia**A survey of the induced seismicity response to fluid injection in geothermal and CO_2 reservoirs in Europe**
Geothermic, 41 (2012), pp. 30-54, 10.1016/j.geothermics.2011.08.002

12. Evans et al., 2005
K.F. Evans, H. Moriya, H. Niitsuma, R.H. Jones, W.S. Phillips, A. Genter, J. Sausse, R. Jung, R. Baria **Microseismicity and permeability enhancement of hydrogeologic structures during massive fluid injections into granite at 3 km depth at the Soultz HDR site**
Geophys. J. Int., 160 (1) (2005), pp. 388-412, 10.1111/j.1365-246X.2004.02474.x

13. Frohlich et al., 2011
C. Frohlich, C. Hayward, B. Stump, E. Potter **The Dallas-for worth earthquake sequence: October 2008 through May 2009**
Bull. Seism. Soc. Am., 101 (2011), pp. 327-340, 10.1785/0120100131

14. Garg and Pritchett, 1984
S.K. Garg, J.W. Pritchett **Pressure transient analysis for two-phase geothermal wells: some numerical results**
Water Resour. Res., 20 (7) (1984), pp. 963-970, 10.1029/WR020i007p00963

15. Gischig and Wiemer, 2013
V. Gischig, S. Wiemer **A stochastic model for induced seismicity based on non-linear pressure diffusion and irreversible permeability enhancement**
Geophys. J. Int., 194 (2) (2013), pp. 1229-1249, 10.1093/gji/ggt164

16. Gischig et al., 2014
V. Gischig, S. Wiemer, A. Alcolea **Balancing reservoir creation and seismic hazard in enhanced geothermal system**

Geophys. J. Int., 198 (2014), pp. 1585-1598, 10.1093/gji/ggu221

17. Goertz-Allmann and Wiemer, 2012
B.P. Goertz-Allmann, S. Wiemer **Geomechanical modeling of induced seismicity source parameters and implications for seismic hazard assessment**
Geophysics, 78 (2012), pp. 25-39, 10.1190/geo2012-0102.1

18. Goertz-Allmann and Wiemer, 2013
B. Goertz-Allmann, S. Wiemer **Geomechanical modeling of induced seismicity source parameters and implications for seismic hazard assessment**
Geophysics, 78 (1) (2013), pp. KS25-KS39, 10.1190/geo2012-0102.1

19. Grünthal, 2014
G. Grünthal **Induced seismicity related to geothermal projects versus natural tectonic earthquakes and other types of induced seismic events in Central Europe**
Geothermics, 52 (2014), pp. 22-35, 10.1016/j.geothermics.2013.09.009

20. Guglielmi et al., 2015
Y. Guglielmi, F. Cappa, J.-P. Avouac, P. Henry, D. Elsworth **Seismicity triggered by fluid injection-induced aseismic slip**
Science, 348 (6240) (2015), pp. 1224-1226, 10.1126/science.aab0476

21. Häring et al., 2008
M. Häring, U. Schanz, F. Ladner, B. Dyer **Characterisation of the Basel enhanced geothermal system**
Geothermics, 37 (2008), pp. 469-495, 10.1016/j.geothermics.2008.06.002

22. Hitzman et al., 2013
Hitzman, M., Clarke, D., Detournay, E., Diederich, J., Dillon, D., Green, S. Habiger, R., McGuire, R., Mitchell, J., Shemeta, J., Smith, J., 2013. Induced Seismicity Potential in Energy Technologies. National Academy of Sciences. The National Academies Press, Washington, D.C., pp. 248.

23. Jeanne et al., 2015
P. Jeanne, J. Rutqvist, A.P. Rinaldi, P.F. Dobson, M. Walters, C. Hartline, J. Garc ia **Seismic and aseismic deformations and impact on reservoir**

permeability: the case of EGS stimulation at The Geysers, California, USA
J. Geophys. Res. – Solid Earth, 120 (2015), pp. 7863-7882, 10.1002/2015JB012142

24. Jha and Juanes, 2014
B. Jha, R. Juanes **Coupled multiphase flow and poromechanics: a computational model of pore pressure effects on fault slip and earthquake triggering**
Water Res. Res., 50 (5) (2014), pp. 3776-3808

25. Karvounis and Wiemer, 2015
Karvounis, D.C., Wiemer, S., 2015. Decision making software for forecasting induced seismicity and thermal energy revenues in enhanced geothermal systems. Proceedings of World Geothermal Congress 2015, Melbourne, Australia, 19–25 April.

26. Keranen et al., 2014
K.M. Keranen, M. Weingartenm, G.A. Abers, B.A. Bekins, S. Ge **Sharp increase in central Oklahoma seismicity since 2008 induced by massive wastewater injection**
Science, 345 (6195) (2014), pp. 448-451, 10.1126/science.1255802

27. Kerr, 2012
Kerr **Learning how to not make your own earthquakes**
Science, 335 (6075) (2012), pp. 1436-1437, 10.1126/science.335.6075.1436

28. King et al., 1994
G.C.P. King, R.S. Stein, J. Lin **Static stress changes and the triggering of earthquakes**
Bull. Seismol. Soc. Am., 84 (1994), pp. 935-953

29. Kiraly et al., 2014
Kiraly, E., Gischig, V., Karvounis, D., Wiemer, S., 2014. Validating models to forecasting induced seismicity related to deep geothermal energy projects, In: Proceedings of the 39th Workshop on Geothermal Reservoir Engineering, Stanford University, Stanford, California, USA, February 24–26, SGP-TR-202.

30. Kolditz et al., 2012

O. Kolditz, S. Bauer, L. Bilke, N. Böttcher, J.O. Delfs, T. Fischer, U.J. Görke, T. Kalbacher, G.Kosakowski, C.I. McDermott, C.H. Park, F. Radu, K. Rink, H. Shao , H.B. Shao, F. Sun, Y.Y. Sun, A.K.Singh, J. Taron, M. Walther, W. Wang, N. Wa tanabe, Y. Wu, M. Xie, W. Xu, B. Zehner **OpenGeoSys: an open-source initiative for numerical simulation of thermo-hydro-mechanical/chemical (THM/C) processes in porous media**
Environ. Earth Sci., 67 (2) (2012), pp. 589-599, 10.1007/s12665-012-1546-x

31. Mazzoldi et al., 2012
A. Mazzoldi, A.P. Rinaldi, J. Rutqvist, A. Borgia **Induced seismicity within geological carbon sequestration projects: maximum earthquake magnitude and leakage potential from undetected faults**
Int. J. Greenh. Gas. Control, 10 (2012), pp. 434-442, 10.1016/j.ijggc.2012.07.012

32. Nicol et al., 2011
A. Nicol, R. Carne, M. Gerstenberger, A. Christophersen **Induced seismicity and its implication for CO_2 storage risk**
Energy Procedia, 4 (2011), pp. 3699-3706, 10.1016/j.egypro.2011.02.302

33. Okada, 1992
Y. Okada **Internal deformation due to shear and tensile faults in a half-space**
Bull. Seism. Soc. Am., 82 (1992), pp. 1018-1040

34. Pruess et al., 2011
Pruess, K., Oldenburg, C.M., Moridis, G., 2011. TOUGH2 User's Guide, Version 2.1, Paper LBNL-43134 (revised). Lawrence Berkeley National Laboratory, Berkeley, CA, USA

35. Rinaldi and Rutqvist, 2013
A.P. Rinaldi, J. Rutqvist **Modeling of deep fracture zone opening and transient ground surface uplift at KB-502 CO_2injection well, In Salah, Algeria**
Int. J. Greenh. Gas. Control, 12 (2013), pp. 155-167, 10.1016/j.ijggc.2012.10.017

36. Rinaldi et al., 2014a

A.P. Rinaldi, J. Rutqvist, F. Cappa **Geomechanical effects on CO_2 leakage through fault zones during large-scale underground injection**
Int. J. Greenh. Gas Control, 20 (2014), p. 171, 10.1016/j.ijggc.2013.11.001

37. Rinaldi et al., 2014b
A.P. Rinaldi, P. Jeanne, J. Rutqvist, F. Cappa, Y. Guglielmi **Effects of fault-zone architecture on earthquake magnitude and gas leakage related to CO_2injection in a multi-layered sedimentary system**
Greenh. Gas. Sci. Technol., 4 (2014), pp. 99-120, 10.1002/ghg.1403

38. Rinaldi et al., 2015a
A.P. Rinaldi, J. Rutqvist, E. Sonnenthal, T.T. Cladouhos **Coupled THM modeling of hydroshearing stimulation in tight fractured volcanic Rock**
Tranp. Porous Med, 108 (1) (2015), pp. 131-150, 10.1007/s11242-014-0296-5

39. Rinaldi et al., 2015b
A.P. Rinaldi, V. Vilarrasa, J. Rutqvist, F. Cappa **Fault reactivation during CO_2 sequestration: effects of well orientation on seismicity and leakage**
Greenh. Gas. Sci. Tech., 5 (2015), pp. 645-656, 10.1002/ghg.1511

40. Rutqvist, 2011
J. Rutqvist **Status of TOUGH-FLAC simulator and recent applications related to coupled fluid flow and crustal deformations**
Comput. Geosci., 37 (2011), pp. 739-750

41. Rutqvist, 2015
J. Rutqvist **Fractured rock stress-permeability relationships from in-situ data and effects of temperature and chemical-mechanical couplings**
Geofluids, 12 (1–2) (2015), pp. 48-66, 10.1111/gfl.12089

42. Samuelson and Spiers, 2012
J. Samuelson, C.J. Spiers **Fault friction and slip stability not affected by CO_2 storage: evidence from short-term laboratory experiments on North Sea reservoir sandstones and caprocks**
Int. J. Greenh. Gas. Contr., 11 (2012), pp. S78-S90, 10.1016/j.ijggc.2012.09.018

43. Schoenball et al., 2012
M. Schoenball, C. Baujard, T. Kohl, L. Dorbath **The role of triggering by static stress transfer during geothermal reservoir stimulation**
J. Geophys. Res., 117 (2012), p. B09307, 10.1029/2012JB009304

44. Scholz, 2015
C.H. Scholz **On the stress dependence of the earthquake *b* value**
Geophys. Res. Lett., 42 (2015), pp. 1399-1402, 10.1002/2014GL062863

45. Shapiro and Dinske, 2009
S.A. Shapiro, C. Dinske **Scaling of seismicity induced by non-linear fluid–rock interaction**
J. Geophys. Res., 114 (B09307) (2009), 10.1029/2008JB006145

46. Shapiro et al., 2010
S.A. Shapiro, C. Dinske, C. Langebruch, F. Wenzel **Seismogenic index and magnitude probability of earthquakes induced during reservoir fluid stimulations**
Lead. Edge – Spec. Sect.: Micro., 29 (3) (2010), pp. 304-309, 10.1190/1.3353727

47. Suckale, 2009
J. Suckale **Induced seismicity in hydrocarbon fields**
Adv. Geophys., 51 (2009), pp. 55-106, 10.1016/S0065-2687(09)05107-3

48. Valley and Evans, 2009
B. Valley, K. Evans **Stress orientation to 5 km depth in the basement below Basel (Switzerland) from borehole failure analysis**
Swiss J., Geosci., 102 (2009), pp. 467-480, 10.1007/s00015-009-1335-z

49. Wells and Coppersmith, 1994
D.L. Wells, K.J. Coppersmith **New empirical relationship among magnitude, rupture length, rupture width, rupture area, and surface displacement**
Bull. Seism. Soc. Am., 84 (1994), pp. 974-1002

50. Zoback, 2010
M.D. Zoback **Reservoir Geomechanics**

Cambridge University Press, New York (2010), p. 449